Available online at www.sciencedirect.com
SCIENCE DIRECT®
Journal of Sound and Vibration 276 (2004) 273–291
JOURNAL OF SOUND AND VIBRATION
www.elsevier.com/locate/jsvi

Optimal control of precision paraboloidal shell structronic systems

H.S. Tzou*, J.H. Ding

Department of Mechanical Engineering, StrucTronics Laboratory, University of Kentucky, Lexington, KY 40506-0503, USA

Received 20 May 2002; accepted 23 July 2003

Abstract

Paraboloidal shells of revolution are commonly used in advanced aerospace, civil and telecommunication structures, e.g., antennas, reflectors, mirrors, rocket fairings, nozzles, solar collectors, dome structures, etc. A structronic shell system is defined as an elastic shell embedded, bonded or laminated with distributed piezoelectric sensors and actuators and it is governed by either in situ or external control electronics. A closed-loop control system of paraboloidal shell structronic system consists of distributed sensors/actuators and controller coupled with an elastic paraboloidal shell. State equation for the paraboloidal shell structronic system is derived and optimal linear quadratic state feedback control is implemented, such that the ''best'' shell control performance with the least control cost can be achieved. The gain matrix is estimated based on minimizing a performance criterion function. Optimal control effects are compared with controlled responses with other non-optimal control parameters. Control effects of identical-sized sensor/actuator patches at different locations are studied and compared. Modal control effects for different natural modes are also investigated.

1. Introduction

Paraboloidal shells of revolution are commonly used in advanced aerospace, civil and telecommunication structures, e.g., antennas, reflectors, mirrors, rocket fairings, nozzles, solar collectors, dome structures, etc. A shell structronic system is defined as an elastic shell bonded, embedded or laminated with active-material-based sensors and actuators governed by either in situ or external control electronics. This study is to apply the linear quadratic (LQ) optimal state feedback control to precision paraboloidal shell structronic systems and to evaluate modal control

*Corresponding author. Tel.: +1-606-257-6336; fax: +1-606-257-3304.
E-mail address: hstzou@engr.uky.edu (H.S. Tzou).

0022-460X/$ - see front matter
doi:10.1016/j.jsv.2003.07.027

effects influenced by different sensor/actuator locations. The goal of optimal control is to seek for the best closed-loop control performance at the least control cost. Although the optimal control technique has been introduced to control applications for decades, its application to shell vibration control, especially distributed structronic shell systems, is still not well explored. Optimal control of distributed parameter systems with spatial and time discretization methods was studied [1], as well as applications to beam and plate structures [2–5]. The dynamic and/or elastic behavior of paraboloidal shells of revolution has been investigated for decades. Lin and Lee [6] derived the mode shape functions and natural frequencies for paraboloidal shells of revolution with free boundary based on the bending approximation. Wang and Lin [7] presented the differential governing equations for the axisymmetric motion of paraboloidal shells of revolution. However, difficulties for finding analytical solutions to the complicated equations of motion limit the fully development and application of elastic paraboloidal shells of revolution. Distributed sensing and control characteristics of structronic beam, plate, ring and shells have been investigated over the years [8–12]. Distributed sensing behaviors and open-loop actuator characteristics of structronic paraboloidal shell of revolution systems were recently investigated [12–14]. In this study, the comprehensive dynamics and closed-loop optimal control performance, with modal-dependent sensor/actuator location sensitivity, of paraboloidal structronic shells (elastic shell coupled with distributed segmented sensors/actuators) are evaluated. Its advantages are demonstrated by comparing the optimal control with the control based on a non-optimal (i.e., proportional and derivative) gain matrix at the same control gain cost.

2. A paraboloidal shell structronic system

The closed-loop active vibration control of paraboloidal shells of revolution structronic system is accomplished by distributed sensors, a controller and distributed actuators, as shown in Fig. 1. The piezoelectric sensor monitors the shell vibration state according to the direct piezoelectric effect. The sensing signal is input to the controller and a control signal is generated based on the sensing signal and the control algorithm. A high-voltage amplifier can be a part of the controller

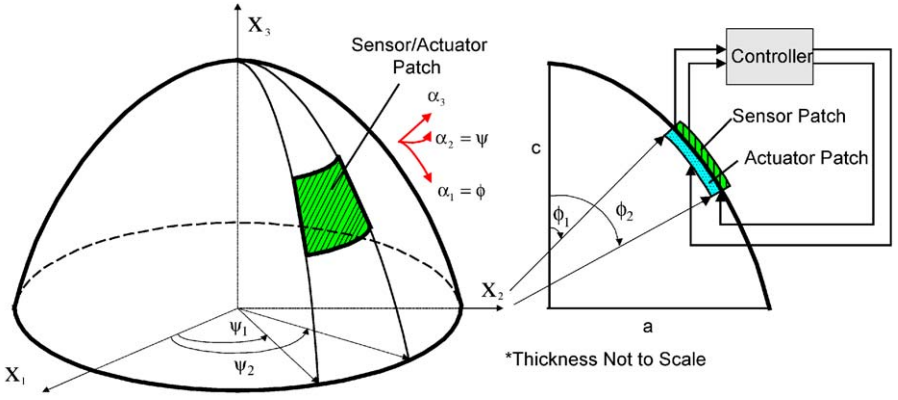

Fig. 1. A closed-loop control system for paraboloidal shell structronic system.

block. The control signal is then transmitted to distributed piezoelectric actuator patches to counteract the shell vibration according to the converse piezoelectric effect.

The tri-orthogonal curvilinear co-ordinates are defined as $\alpha_1 = \phi$—the meridional direction, $\alpha_2 = \psi$—the circumferential direction and α_3—the transverse direction following the right-hand rule (Fig. 1). $R_1 = R_\phi$ is the radius of meridional curvature, $R_2 = R_\psi$ is the radius of circumferential curvature. The radii of curvature of paraboloidal shells of revolution are $R_\psi = b/\cos\phi$ and $R_\phi = b/\cos^3\phi$. The Lamé parameters are $A_1 = R_\phi = b/\cos^3\phi$ and $A_2 = R_\psi \sin\phi = b\sin\phi/\cos\phi$, where $b = a^2/(2c)$, a is the maximum circumferential radius and c is the meridian height (Fig. 1) [13]. State-space equations and optimal control are discussed next.

3. System equation in state space

The fundamental equations of motion for a shell of revolution are [8]:

$$R_\phi \frac{\partial}{\partial\psi}(N_{\psi\phi}) + \frac{\partial}{\partial\phi}(N_{\phi\phi}R_\psi \sin\phi) - N_{\psi\psi}R_\phi \cos\phi + R_\phi R_\psi \sin\phi\left(\frac{Q_{\phi 3}}{R_\phi} + q_\phi\right) = R_\phi R_\psi \sin\phi\, \rho h \frac{\partial^2 u_\phi}{\partial t^2}, \tag{1}$$

$$R_\phi \frac{\partial}{\partial\psi}(N_{\psi\psi}) + \frac{\partial}{\partial\phi}(N_{\phi\psi}R_\psi \sin\phi) + N_{\psi\phi}R_\phi \cos\phi + R_\phi R_\psi \sin\phi\left(\frac{Q_{\psi 3}}{R_\psi} + q_\psi\right) = R_\phi R_\psi \sin\phi\, \rho h \frac{\partial^2 u_\psi}{\partial t^2}, \tag{2}$$

$$R_\phi \frac{\partial}{\partial\psi}(Q_{\psi 3}) + \frac{\partial}{\partial\phi}(Q_{\phi 3}R_\psi \sin\phi) - \left(\frac{N_{\phi\phi}}{R_\phi} + \frac{N_{\psi\psi}}{R_\psi}\right)R_\phi R_\psi \sin\phi + q_3 R_\phi R_\psi \sin\phi = R_\phi R_\psi \sin\phi\, \rho h \frac{\partial^2 u_3}{\partial t^2}, \tag{3}$$

where N_{ij} and M_{ij} are the membrane forces and the bending moments; ρ is the shell mass density; h is the thickness; q_i and u_i are, respectively, the excitation (loading) and displacement in the i direction ($i = \phi, \psi, 3$); and the transverse shear effects Q_{i3} are

$$Q_{\phi 3} = \frac{1}{R_\phi R_\psi \sin\phi}\left[R_\phi \frac{\partial}{\partial\psi} M_{\psi\phi} + \frac{\partial}{\partial\phi}(M_{\phi\phi}R_\psi \sin\phi) - M_{\psi\psi}R_\phi \cos\phi\right], \tag{4}$$

$$Q_{\psi 3} = \frac{1}{R_\phi R_\psi \sin\phi}\left[R_\phi \frac{\partial}{\partial\psi} M_{\psi\psi} + \frac{\partial}{\partial\phi}(M_{\psi\phi}R_\psi \sin\phi) + M_{\psi\phi}R_\phi \cos\phi\right]. \tag{5}$$

Substituting the radii of curvature and force/moment expressions into the fundamental equation of motion and imposing the bending approximation yields the transverse oscillation equation of

paraboloidal shells:

$$
\begin{aligned}
&D\frac{\partial^3 u_\phi}{\partial\phi^3}\left[\frac{\cos^8\phi\sin^3\phi}{b^2}\right]+D\frac{\partial^2 u_\phi}{\partial\phi^2}\left[\frac{-16\cos^7\phi+34\cos^9\phi-18\cos^{11}\phi}{b^2}\right]\\
&\quad+D\frac{\partial u_\phi}{\partial\phi}\left[\frac{(67\cos^6\phi-234\cos^8\phi+266\cos^{10}\phi-99\cos^{12}\phi)-\mu\cos^6\phi\sin^4\phi}{b^2\sin\phi}\right]\\
&\quad+D\frac{\partial^2 u_\phi}{\partial\psi^2}\left[\frac{-2\cos^3\phi+3\cos^5\phi}{b^2}\right]+D\frac{\partial^3 u_\phi}{\partial\phi\partial\psi^2}\left[\frac{\cos^4\phi\sin^2\phi}{b^2\sin\phi}\right]\\
&\quad+Du_\phi\left[\frac{(-66\cos^5\phi+295\cos^7\phi-390\cos^9\phi+162\cos^{11}\phi)}{b^2}\right.\\
&\qquad\left.+\frac{\mu(6\cos^5\phi-13\cos^7\phi+7\cos^9\phi)}{b^2}\right]\\
&\quad+D\frac{\partial^3 u_\psi}{\partial\psi^3}\left[\frac{1}{b^2}\right]+D\frac{\partial u_\psi}{\partial\psi}\left[\frac{(7\cos^2\phi-10\cos^4\phi+4\cos^6\phi)-\mu\cos^2\phi\sin^2\phi}{b^2\sin\phi}\right]\\
&\quad+D\frac{\partial^3 u_\psi}{\partial\psi\partial\phi^2}\left[\frac{\cos^4\phi\sin^2\phi}{b^2}\right]+D\frac{\partial^2 u_\psi}{\partial\phi\partial\psi}\left[\frac{-6\cos^3\phi+11\cos^5\phi-5\cos^7\phi}{b^2\sin\phi}\right]\\
&\quad+D\frac{\partial^4 u_3}{\partial\phi^4}\left[\frac{-\cos^8\phi\sin^4\phi}{b^2\sin\phi}\right]+D\frac{\partial^3 u_3}{\partial\phi^3}\left[\frac{16\cos^7\phi-34\cos^9\phi+18\cos^{11}\phi}{b^2}\right]\\
&\quad+D\frac{\partial^2 u_3}{\partial\phi^2}\left[\frac{(-67\cos^6\phi+234\cos^8\phi-266\cos^{10}\phi+99\cos^{12}\phi)+\mu\cos^6\phi\sin^4\phi}{b^2\sin\phi}\right]\\
&\quad+D\frac{\partial u_3}{\partial\phi}\left[\frac{(66\cos^5\phi-295\cos^7\phi+390\cos^9\phi-162\cos^{12}\phi)}{b^2}\right.\\
&\qquad\left.-\frac{\mu(6\cos^5\phi-13\cos^7\phi+7\cos^9\phi)}{b^2}\right]\\
&\quad+D\frac{\partial^4 u_3}{\partial\psi^4}\left[\frac{-1}{b^2\sin\phi}\right]+D\frac{\partial^2 u_3}{\partial\psi^2}\left[\frac{(-7\cos^2\phi+3\cos^4\phi)+\mu\cos^2\phi\sin^2\phi}{b^2\sin\phi}\right]\\
&\quad+D\frac{\partial^4 u_3}{\partial\phi^2\partial\psi^2}\left[\frac{-2\cos^4\phi+2\cos^6\phi}{b^2\sin\phi}\right]+D\frac{\partial^3 u_3}{\partial\phi\partial\psi^2}\left[\frac{8\cos^3\phi-6\cos^5\phi}{b^2}\right]+q_3\left[\frac{b^2\sin^3\phi}{\cos^4\phi}\right]\\
&=\frac{\partial^2 u_3}{\partial t^2}\left[\frac{b^2\rho h\sin^3\phi}{\cos^4\phi}\right],
\end{aligned}
\tag{6}
$$

where D is the bending stiffness. Furthermore, the modal expansion method [15] is used in the optimal control and the distributed sensing/control analysis of paraboloidal shells [8]. Thus, the modal expansion equation can be written as

$$
u_i(\phi,\psi,t)=\sum_{m=2}^{\infty}\eta_m(t)U_{im}(\phi,\psi),
\tag{7}
$$

where $i = \phi, \psi, 3$ denote for the three co-ordinates; $\eta_m(t)$ is the modal participating factor of the mth mode; $U_{im}(\phi, \psi)$ is the mth mode shape function of a free-floating paraboloidal shell [6]:

$$U_{\phi_m} = -A_m \sin\phi \tan^m\phi \cos m\psi, \tag{8}$$

$$U_{\psi_m} = -A_m \tan^{m+1}\phi \sin m\psi, \tag{9}$$

$$U_{3m} = A_m \tan^m \phi(\cos\phi + m\sec\phi)\cos m\psi, \tag{10}$$

where A_m is the modal amplitude. Note that for paraboloidal shells of revolution with free boundary, the mode number m is the circumferential wave number starting from 2, based on the bending approximation theory [6]. The modal equation can be written as [8]

$$\ddot{\eta}_m + 2\varsigma_m\omega_m\dot{\eta}_m + \omega_m^2\eta_m = \hat{F}_m(t), \tag{11}$$

where ς_m is the modal damping ratio, ω_m is the mth natural frequency, $\hat{F}_m(t)$ is the modal force. In practical implementation, the modal signal can be spectrally decomposed from the sensor signal using band-pass filters or digital filters in conjunction with a fast Fourier transform (FFT). The total closed-loop control system can be divided into a number of subsystems (modal loops) designed for various natural modes. The final total control signal can be reconstructed by re-composing all actuating signals from the subsystems [16]. Note that the spatial derivatives are with respect to the mode shape functions and the temporal derivative is with respect to the modal participating factor when both the mode shape functions and the modal expansion equation are substituted into the transverse shell equation, (6). Accordingly, the shell transverse equation of motion for the mth mode can be written as

$$\begin{aligned}
\eta_m(t)D\Bigg\{&\frac{\partial^3 U_{\phi m}}{\partial\phi^3}\left[\frac{\cos^8\phi\sin^3\phi}{b^2}\right] + \frac{\partial^2 U_{\phi m}}{\partial\phi^2}\left[\frac{-16\cos^7\phi + 34\cos^9\phi - 18\cos^{11}\phi}{b^2}\right]\\
&+ \frac{\partial U_{\phi m}}{\partial\phi}\left[\frac{(67\cos^6\phi - 234\cos^8\phi + 266\cos^{10}\phi - 99\cos^{12}\phi) - \mu\cos^6\phi\sin^4\phi}{b^2\sin\phi}\right]\\
&+ \frac{\partial^2 U_{\phi m}}{\partial\psi^2}\left[\frac{-2\cos^3\phi + 3\cos^5\phi}{b^2}\right] + \frac{\partial^3 U_{\phi m}}{\partial\phi\partial\psi^2}\left[\frac{\cos^4\phi\sin^2\phi}{b^2\sin\phi}\right]\\
&+ U_{\phi m}\left[\frac{(-66\cos^5\phi + 295\cos^7\phi - 390\cos^9\phi + 162\cos^{11}\phi)}{b^2}\right.\\
&\qquad\left.+ \frac{\mu(6\cos^5\phi - 13\cos^7\phi + 7\cos^9\phi)}{b^2}\right]\\
&+ \frac{\partial^3 U_{\psi m}}{\partial\psi^3}\left[\frac{1}{b^2}\right] + \frac{\partial U_{\psi m}}{\partial\psi}\left[\frac{(7\cos^2\phi - 10\cos^4\phi + 4\cos^6\phi) - \mu\cos^2\phi\sin^2\phi}{b^2}\right]\\
&+ \frac{\partial^3 U_{\psi m}}{\partial\phi^2\partial\psi}\left[\frac{\cos^4\phi\sin^2\phi}{b^2}\right] + \frac{\partial^2 U_{\psi m}}{\partial\phi\partial\psi}\left[\frac{-6\cos^3\phi + 11\cos^5\phi - 5\cos^7\phi}{b^2\sin\phi}\right]
\end{aligned}$$

$$
\begin{aligned}
&+\frac{\partial^4 U_{3m}}{\partial\phi^4}\left[\frac{-\cos^8\phi\sin^3\phi}{b^2}\right]+\frac{\partial^3 U_{3m}}{\partial\phi^3}\left[\frac{16\cos^7\phi-34\cos^9\phi+18\cos^{11}\phi}{b^2}\right]\\
&+\frac{\partial^2 U_{3m}}{\partial\phi^2}\left[\frac{(-67\cos^6\phi+234\cos^8\phi-266\cos^{10}\phi+99\cos^{12}\phi)+\mu\cos^6\phi\sin^4\phi}{b^2\sin\phi}\right]\\
&+\frac{\partial U_{3m}}{\partial\phi}\left[\frac{66\cos^5\phi-295\cos^7\phi+390\cos^9\phi-162\cos^{11}\phi}{b^2}\right.\\
&\qquad\left.-\frac{\mu(6\cos^5\phi-13\cos^7\phi+7\cos^9\phi)}{b^2}\right]\\
&+\frac{\partial^4 U_{3m}}{\partial\psi^4}\left[\frac{-1}{b^2\sin\phi}\right]+\frac{\partial^2 U_{3m}}{\partial\psi^2}\left[\frac{(-7\cos^2\phi+3\cos^4\phi)+\mu\cos^2\phi\sin^2\phi}{b^2\sin\phi}\right]\\
&+\frac{\partial^4 U_{3m}}{\partial\phi^2\partial\psi^2}\left[\frac{-2\cos^4\phi\sin\phi}{b^2}\right]+\frac{\partial^3 U_{3m}}{\partial\phi\partial\psi^2}\left[\frac{8\cos^3\phi-6\cos^5\phi}{b^2}\right]\Bigg\}+q_{3m}\left[\frac{b^2\sin^3\phi}{\cos^4\phi}\right]\\
&=\frac{\mathrm{d}^2\eta_m(t)}{\mathrm{d}t^2}U_{3m}\left[\frac{b^2\rho h\sin^3\phi}{\cos^4\phi}\right],
\end{aligned}
\tag{12}
$$

where q_{3m} is the modal excitation. This equation is further transferred into the state-space, since the state-space formulation is the fundamental in modern control techniques. Here, the modal participating factor $\eta_m(t)$ and its time derivative $\dot{\eta}_m(t)$ are chosen to be the system state variables and the equation of motion is rewritten into the state-space form as $\dot{\mathbf{x}}=\mathbf{A}\mathbf{x}+\mathbf{B}\mathbf{u}+\mathbf{E}\mathbf{w}$ and $\mathbf{y}=\mathbf{C}\mathbf{x}$, where $\mathbf{x}$ is the state-variable vector; $\mathbf{u}$ is the control input vector; $\mathbf{w}$ is external excitation (disturbance); $\mathbf{y}$ is the output vector; $\mathbf{A}$, $\mathbf{B}$, $\mathbf{C}$ and $\mathbf{E}$ are known coefficient matrices related to the system state, control input, system output and excitation input, respectively. The system state is defined as

$$
\mathbf{x}=\begin{Bmatrix}x_1\\x_2\end{Bmatrix}=\begin{Bmatrix}\eta_m(t)\\\dot{\eta}_m(t)\end{Bmatrix}. \tag{13}
$$

$\eta_m(t)$ represents the modal displacement of the shell and $\dot{\eta}_m(t)$ represents the modal velocity. The system state equation is

$$
\begin{Bmatrix}\dot{\eta}_m(t)\\\ddot{\eta}_m(t)\end{Bmatrix}=\begin{bmatrix}A_{11}&A_{12}\\A_{21}&A_{22}\end{bmatrix}\begin{Bmatrix}\eta_m(t)\\\dot{\eta}_m(t)\end{Bmatrix}+\begin{Bmatrix}B_1\\B_2\end{Bmatrix}\hat{F}_m^c(t)+\begin{Bmatrix}E_1\\E_2\end{Bmatrix}q_{3m}(t). \tag{14}
$$

The system output is chosen to be the sensing signal ϕ_m^s, so the output equation is

$$
\phi_m^s=[C_1\quad C_2]\begin{Bmatrix}\eta_m(t)\\\dot{\eta}_m(t)\end{Bmatrix}=[C_1\quad 0]\begin{Bmatrix}\eta_m(t)\\\dot{\eta}_m(t)\end{Bmatrix}=C_1\eta_m(t). \tag{15}
$$

$\mathbf{A}$, $\mathbf{B}$ and $\mathbf{E}$ are the coefficient matrices determined by Eqs. (11) and (12); $\mathbf{C}$ can be determined by the distributed sensing characteristic of free-boundary paraboloidal shell. The modal control force $\hat{F}_m^c(t)$ is the control input and the system state, i.e., the modal displacement and velocity, is the

feedback signal in the closed-loop control system. For a linear control law,

$$\hat{F}_m^c(t) = -\mathbf{G}\mathbf{x}(t) = -\mathbf{G}\{\eta_m(t) \quad \dot{\eta}_m(t)\}^{\mathrm{t}}. \tag{16}$$

In practical applications, the control gain $\mathbf{G}$ is usually referred to the ratio between the control signal and the sensing signal:

$$\phi_m^a = -\mathbf{G}^*\{\phi_m^s \quad \dot{\phi}_m^s\}^{\mathrm{t}}, \tag{17}$$

where $\mathbf{G}^*$ is the gain that relates the control signal to the sensing signal. The relation between $\mathbf{G}^*$ and the theoretical control gain $\mathbf{G}$ in Eq. (16) can be estimated based on the system equations and the modal control force analysis. Note that the velocity signal can be measured directly by velocity sensors, or it can be acquired by differentiating the displacement signal. In practice, to avoid the differentiation process amplified noises, appropriate filter selection to keep the signal at a good signal noise ratio (SNR) is required. Furthermore, the closed-loop system equation without external excitation is simplified to $\dot{\mathbf{x}} = \mathbf{A}\mathbf{x} - \mathbf{B}\mathbf{G}\mathbf{x} = \mathbf{A}_c\mathbf{x}$, where $\mathbf{A}_c$ is the closed-loop system state coefficient matrix. When all system matrices are time-invariant, the solution is

$$\mathbf{x}(t) = \mathrm{e}^{\mathbf{A}_c(t-t_0)}\mathbf{x}(t_0), \tag{18}$$

where "t" is any time instant after the initial time t_0; $\mathbf{x}(t_0)$ is the system initial state.

4. Optimal gain matrix

The criterion function of LQ optimal control is the integration of the quadratic form of the state $\mathbf{x}$ plus a second quadratic form of the control $\mathbf{u}$ [17]:

$$J = \int_{t_0}^{T} [\mathbf{x}^{\mathrm{t}}(t)\mathbf{Q}(t)\mathbf{x}(t) + \mathbf{u}^{\mathrm{t}}(t)\mathbf{R}\mathbf{u}(t)]\,\mathrm{d}t, \tag{19}$$

where $\mathbf{x}$ is the system state; $\mathbf{Q}$ is the state weighting matrix and $\mathbf{R}$ is the control weighting matrix (both are positive symmetric matrices); t_0 is the initial time, T is the final time; the superscript "t" denotes the matrix/vector transpose here. Weighting matrices are chosen based on the desired control cost and final control performance. The optimal control gain is searched to minimize this criterion function and is found by $\hat{\mathbf{G}} = \mathbf{R}^{-1}\mathbf{B}^{\mathrm{t}}\hat{\mathbf{M}}$, where the matrix $\hat{\mathbf{M}}$ is the solution of the matrix Riccati equation in the modern control theory [16]:

$$-\dot{\hat{\mathbf{M}}} = \hat{\mathbf{M}}\mathbf{A} + \mathbf{A}^{\mathrm{t}}\hat{\mathbf{M}} - \hat{\mathbf{M}}\mathbf{B}\mathbf{R}^{-1}\mathbf{B}^{\mathrm{t}}\hat{\mathbf{M}} + \mathbf{Q}. \tag{20}$$

If the interval time goes to infinit ($T \to \infty$) and $J_\infty = \int_0^\infty (\mathbf{x}^{\mathrm{t}}\mathbf{Q}\mathbf{x} + \mathbf{u}^{\mathrm{t}}\mathbf{R}\mathbf{U})\,\mathrm{d}t$ converges, the gain matrix can be a constant and is called the optimal gain in the steady state, noted as

$$\bar{\mathbf{G}} = \mathbf{R}^{-1}\mathbf{B}^{\mathrm{t}}\bar{\mathbf{M}}. \tag{21}$$

Then matrix $\bar{\mathbf{M}}$ is the solution to

$$0 = \bar{\mathbf{M}}\mathbf{A} + \mathbf{A}^{\mathrm{t}}\bar{\mathbf{M}} - \bar{\mathbf{M}}\mathbf{B}\mathbf{R}^{-1}\mathbf{B}^{\mathrm{t}}\bar{\mathbf{M}} + \mathbf{Q}. \tag{22}$$

Note that $\bar{\mathbf{M}}$ is related to the optimal gain in the steady state optimal gain $\bar{\mathbf{G}}$ and $\hat{\mathbf{M}}$ is related to the generic optimal gain $\hat{\mathbf{G}}$. For the paraboloidal shell structronic system, the coefficient matrices

are

$$\mathbf{A} = \begin{bmatrix} 0 & 1 \\ A_{21} & A_{22} \end{bmatrix}, \quad \mathbf{B} = \begin{bmatrix} 0 \\ 1 \end{bmatrix}.$$

The state weighting matrix is chosen as

$$\mathbf{Q} = \begin{bmatrix} 1 & 0 \\ 0 & c^2 \end{bmatrix},$$

where c is a state weighting coefficient. The control weighting matrix $\mathbf{R}$ is now simplified to a single parameter R as the control input is only $\hat{F}_m^c$, not a vector. $\bar{\mathbf{M}}$ is a symmetric matrix due to its definition [16],

$$\bar{\mathbf{M}} = \begin{bmatrix} m_1 & m_2 \\ m_2 & m_3 \end{bmatrix}$$

and it is found that

$$m_2 = R(A_{21} \pm \sqrt{A_{21}^2 + 1/R}), \quad m_3 = R[A_{22} \pm \sqrt{A_{22}^2 + (2m_2 + c^2)/R}]. \tag{23a, b}$$

Since m_1 is not used in the gain calculation, it is not calculated. Thus, the optimal matrix $\bar{\mathbf{G}}$ is determined by Eq. (20) as

$$\bar{\mathbf{G}} = [A_{21} + \sqrt{A_{21}^2 + 1/R} \quad A_{22} + \sqrt{A_{22}^2 + (2m_2 + c^2)/R}]. \tag{24}$$

These coefficients are defined by $A_{12} = 1$, $A_{22} = -2\varsigma_m\sqrt{-A_{21}}$, and

$$\begin{aligned} A_{21} = {} & \frac{D\cos^4\phi}{U_{3m}b^4\rho h\sin^4\phi}\left\{\frac{\partial^3 U_{\phi m}}{\partial\phi^3}[\cos^8\phi\sin^4\phi]\right. \\ & + \frac{\partial^2 U_{\phi m}}{\partial\phi^2}[(-16\cos^7\phi + 34\cos^9\phi - 18\cos^{11}\phi)\sin\phi] \\ & + \frac{\partial U_{\phi m}}{\partial\phi}[(67\cos^6\phi - 234\cos^8\phi + 266\cos^{10}\phi - 99\cos^{12}\phi) - \mu\cos^6\phi\sin^4\phi] \\ & + \frac{\partial^2 U_{\phi m}}{\partial\psi^2}[(-2\cos^3\phi + 3\cos^5\phi)\sin\phi] + \frac{\partial^3 U_{\phi m}}{\partial\phi\partial\psi^2}[\cos^4\phi\sin^2\phi] \\ & + U_{\phi m}[(-66\cos^5\phi + 295\cos^7\phi - 390\cos^9\phi + 162\cos^{11}\phi)\sin\phi \\ & \qquad + \mu(6\cos^5\phi - 13\cos^7\phi + 7\cos^9\phi)\sin\phi] \\ & + \frac{\partial^3 U_{\psi m}}{\partial\psi^3}[\sin\phi] + \frac{\partial U_{\psi m}}{\partial\psi}[(7\cos^2\phi - 10\cos^4\phi + 4\cos^6\phi)\sin\phi - \mu\cos^2\phi\sin^3\phi] \\ & + \frac{\partial^3 U_{\psi m}}{\partial\phi^2\partial\psi}[\cos^4\phi\sin^3\phi] + \frac{\partial^2 U_{\psi m}}{\partial\phi\partial\psi}[-6\cos^3\phi + 11\cos^5\phi - 5\cos^7\phi] \\ & \left. + \frac{\partial^4 U_{3m}}{\partial\phi^4}[-\cos^8\phi\sin^4\phi] + \frac{\partial^3 U_{3m}}{\partial\phi^3}[(16\cos^7\phi - 34\cos^9\phi + 18\cos^{11}\phi)\sin\phi]\right. \end{aligned}$$

$$+\frac{\partial^2 U_{3m}}{\partial\phi^2}[(-67\cos^6\phi+234\cos^8\phi-266\cos^{10}\phi+99\cos^{12}\phi)+\mu\cos^6\phi\sin^4\phi]$$
$$+\frac{\partial U_{3m}}{\partial\phi}[(66\cos^5\phi-295\cos^7\phi+390\cos^9\phi-162\cos^{11}\phi)\sin\phi$$
$$-\mu(6\cos^5\phi-13\cos^7\phi+7\cos^9\phi)\sin\phi]$$
$$-\frac{\partial^4 U_{3m}}{\partial\psi^4}+\frac{\partial^2 U_{3m}}{\partial\psi^2}[(-7\cos^2\phi+3\cos^4\phi)+\mu\cos^2\phi\sin^2\phi]$$
$$+\frac{\partial^4 U_{3m}}{\partial\phi^2\partial\psi^2}[-2\cos^4\phi\sin^2\phi]+\frac{\partial^3 U_{3m}}{\partial\phi\partial\psi^2}[(8\cos^3\phi-6\cos^5\phi)\sin\phi]\Big\}. \quad (25)$$

Application of the algorithm to the optimal control of paraboloidal shell structronic system is demonstrated next.

5. Case studies

Optimal vibration control of a paraboloidal shell structronic system with free boundary is studied; control sensitivities at various sensor/actuator locations are evaluated. The maximum circumferential radius of the shell is $a = 1$ m, height $c = 1$ m and thickness $h = 0.1$ m, shown in Fig. 2. The shell is made of Plexiglas and the piezoelectric sensor/actuator patches are polyvinylidene-fluoride (PVDF) films. The geometry and material properties are summarized in Table 1. Three sensor/actuator locations are studied, i.e., Location 1: $(\phi,\psi)=(0.85,0.1)$, Location 2: $(\phi,\psi)=(0.95,0.1)$ and Location 3: $(\phi,\psi)=(1.05,0.1)$, all in radians. The circumferential widths of the sensor/actuator patches at the three locations are $\psi = 0$–0.2 rad to exclude the influence of the circumferential wave and these three sensor/actuator patches are of identical sizes, i.e., 0.03628 m^2. The meridional co-ordinates of the patches at the three locations are Location 1: $\phi = 0.76262$–0.93738 rad, Location 2: $\phi = 0.9$–1.0 rad and Location 3: $\phi = 1.024565$–1.075435 rad. Note that the 1st patch (Location 1) slightly overlaps the 2nd patch (Location 2) in order to keep the same circumferential co-ordinate and thus, the same size.

Weighting matrices in the optimal control are chosen based on the control performance and the desired control gain cost. (Too large feedback gain is impractical due to physical limitations, although it might provide a better control performance.) The total gain cost of $\mathbf{G}^*$ $(G_1^* + G_2^*)$ is assumed to be 300. In order to be compatible with the PD control with $\mathbf{G}^* = [200, 100]$, the total gain cost for the optimal control gain $\bar{\mathbf{G}}$ is also chosen to be 300. (Note that the exact estimated results from the optimal control algorithm are between 299 and 300 and the gain mentioned here is referred to the ratio between the actuation signal and the sensing signal.) The control input weighting coefficient R is chosen to be 1 for all the optimal control studied here and the state weighting coefficient c is adjusted to achieve the desired gain cost. The optimal gain matrix $\bar{\mathbf{G}}$ calculated from the optimal control algorithm indicates that the second entry $\bar{\mathbf{G}}_2$ is dominant, i.e., the gain cost is mostly assigned to the gain related to the second state variable—the derivative component $\dot{\eta}_m$ (i.e., the modal velocity).

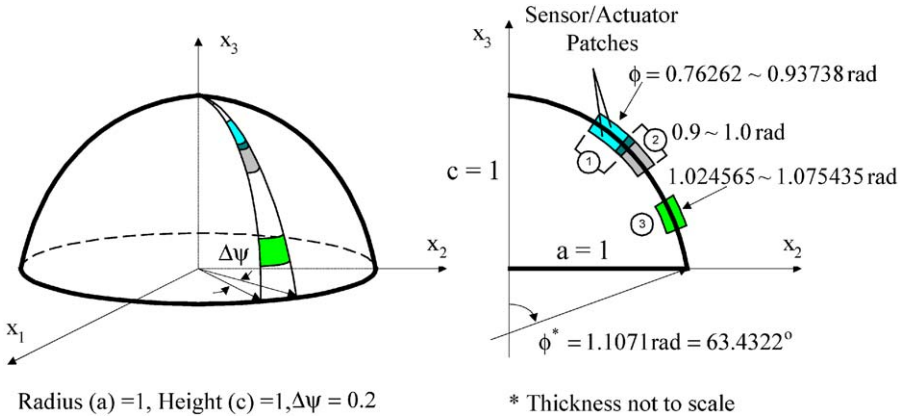

Fig. 2. A paraboloidal shell with sensor/actuator patches at three locations.

Table 1
Geometry and material properties of the structronic paraboloidal shell system

Properties	PVDF layer	Plexiglas shell	Units
Circumferential radius		$a = 1$	m
Meridional height		$c = 1$	m
Thickness	$h^s = h^a = 5 \times 10^{-4}$	$h = 0.10$	m
Young's modulus	$Y_p = 2.00 \times 10^9$	$Y = 3.1028 \times 10^9$	N/m^2
Mass density	$\rho_p = 1800.0$	$\rho = 1190.0$	kg/m^3
The Poisson ratio		$\mu = 0.3$	
Bending stiffness		$D = 2.8414 \times 10^5$	N m
Membrane stiffness		$K = 3.4097 \times 10^8$	N m
Piezoelectric constants	$h_{31} = 4.32 \times 10^8$		$\frac{V/m}{m/m}$
	$d_{31} = 2.3 \times 10^{-11}$		$\frac{m/m}{V/m}$

Time-history responses of the center of the sensor/actuator patches at three shell locations are investigated, to which an initial displacement 0.001 m with zero initial velocity is imposed. Note the initial displacement and velocity need to be converted to the initial system state $\mathbf{x}(t_0) = \{\eta(t_0)\ \dot{\eta}(t_0)\}^t$ in the modal domain. Initial modal damping ratio of free vibrations is assumed to be 0.002 and the modal amplitude A_m is set unity. Numerical time steps of the time-history responses are 1000. For comparison, time-histories of the optimal control, free vibration, and the state feedback control using a non-optimal gain, i.e., $\mathbf{G}^* = [200, 100]$, of the ($m = 2$–6) paraboloidal shell modes at the three sensor/actuator locations are studied and only the ($m = 2$–4) responses are presented in Figs. 3–11. Localized dynamic and control characteristics contribute to the differences among these time histories. Time histories of the free and control responses are further processed to calculate their inferred equivalent modal damping ratios ($m = 2$–6) at these three sensor/actuator locations, resulting from the optimal control ($\bar{\mathbf{G}}$) and the PD control ($\mathbf{G}^*$). Fig. 12 shows the damping ratio variation for the five shell modes ($m = 2$–6); Fig. 13 shows the damping ratio variation at three sensor/actuator locations.

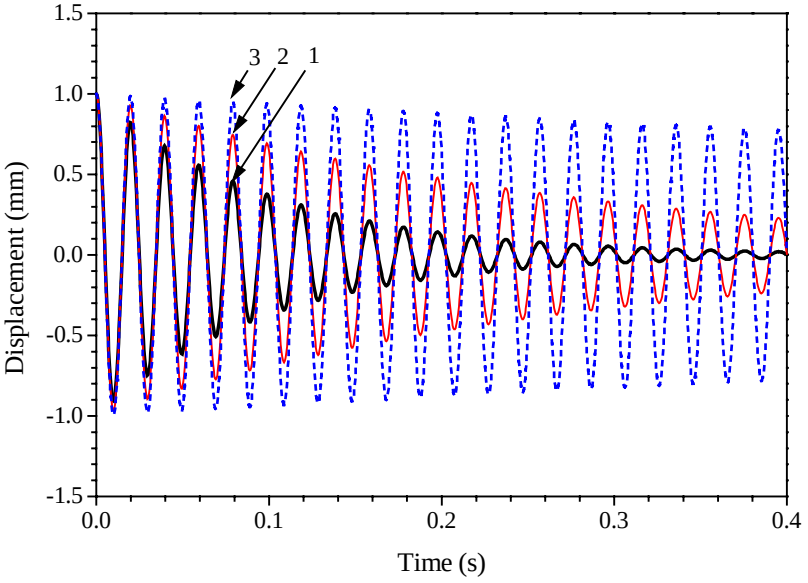

Fig. 3. Control with sensor/actuator at Location 1, $m = 2$: 1, optimal control ($\bar{\mathbf{G}}$); 2, control ($\mathbf{G}^*$); 3, free vibration; $\mathbf{G}^* = [200, 100]$, $\bar{\mathbf{G}} = [8.041272\text{E}{-}05, 299.647600]$, time step = 0.4 ms.

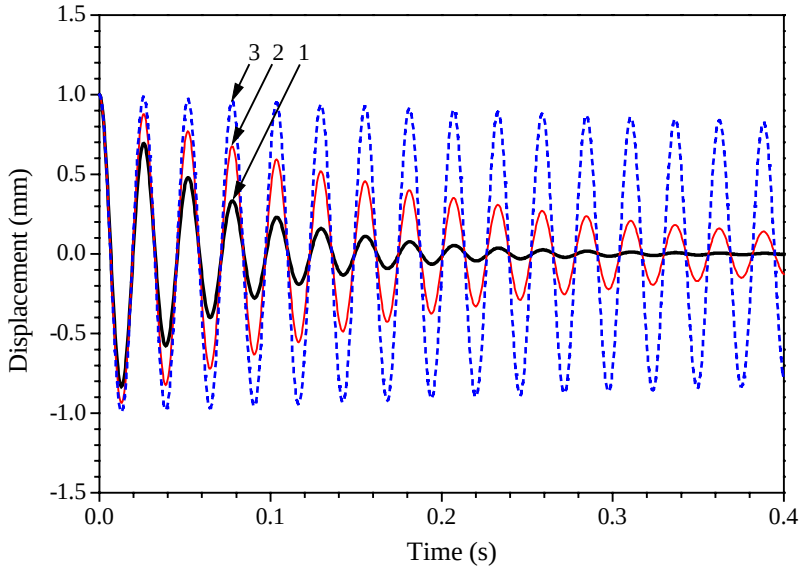

Fig. 4. Control with sensor/actuator at Location 2, $m = 2$: 1, optimal control ($\bar{\mathbf{G}}$); 2, control ($\mathbf{G}^*$); 3, free vibration; $\mathbf{G}^* = [200, 100]$, $\bar{\mathbf{G}} = [9.281180\text{E}{-}05, 299.290900]$, time step = 0.4 ms.

These time-history responses clearly reveal that the optimal control is superior to the PD control. However, this control effect reduces at high natural modes, because the oscillation amplitude is usually small; so are the sensing and control signals when control gains are fixed.

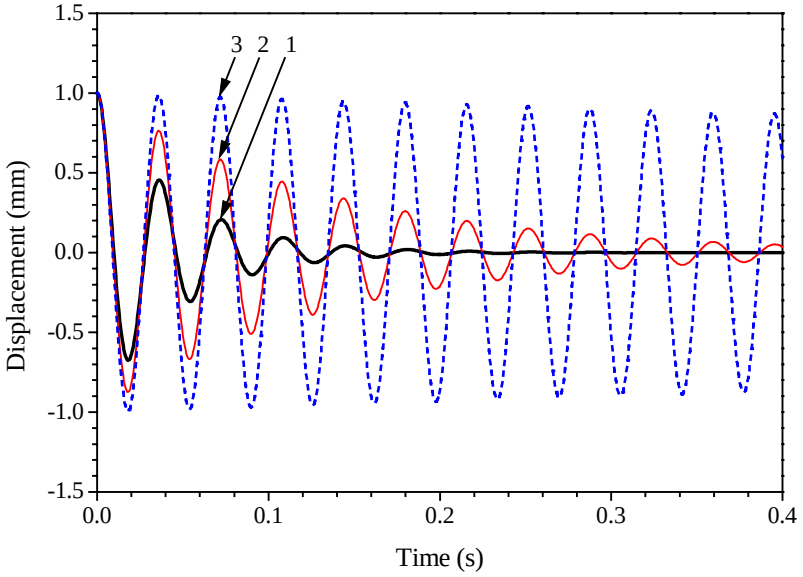

Fig. 5. Control with sensor/actuator at Location 3, $m = 2$: 1, optimal control ($\bar{\mathbf{G}}$); 2, control ($\mathbf{G}^*$); 3, free vibration, $\mathbf{G}^* = [200, 100]$, $\bar{\mathbf{G}} = [1.144451\text{E}{-}04, 299.959400]$, time step = 0.4 ms.

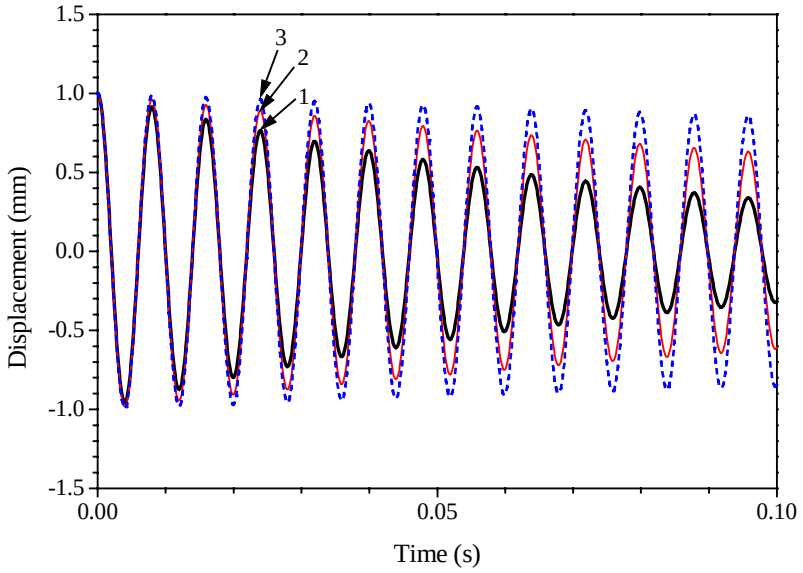

Fig. 6. Control with sensor/actuator at Location 1, $m = 3$: 1, optimal control ($\bar{\mathbf{G}}$); 2, control ($\mathbf{G}^*$); 3, free vibration; $\mathbf{G}^* = [200, 100]$, $\bar{\mathbf{G}} = [1.244259\text{E}{-}05, 299.959700]$, time step = 0.1 ms.

Since the gain estimation involves a specific location and its meridional/circumferential angles of the sensor/actuator patches, the time-history responses at these three locations reveal variations of oscillation frequencies. The coefficients in the system equation and the meridional radii of

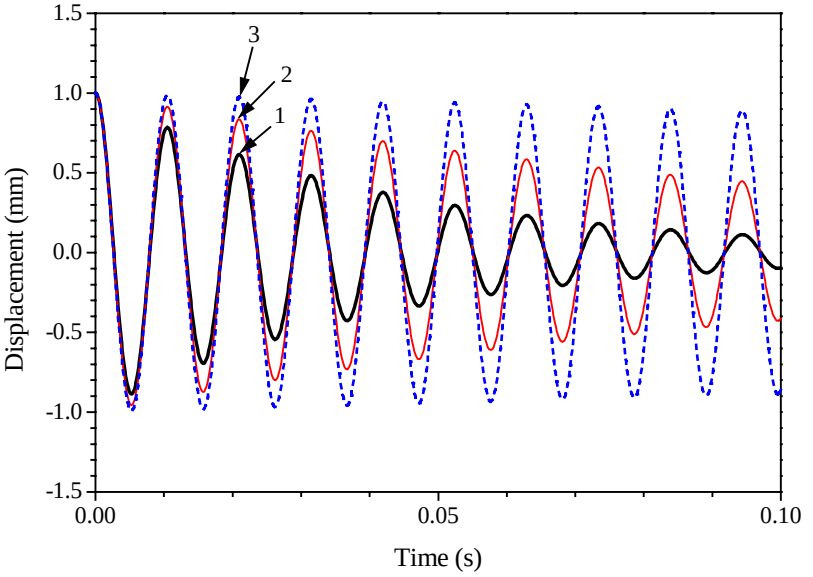

Fig. 7. Control with sensor/actuator at Location 2, $m = 3$: 1, optimal control ($\bar{\mathbf{G}}$); 2, control ($\mathbf{G}^*$); 3, free vibration; $\mathbf{G}^* = [200, 100]$, $\bar{\mathbf{G}} = [9.475585\text{E–}06, 299.426500]$, time step = 0.1 ms.

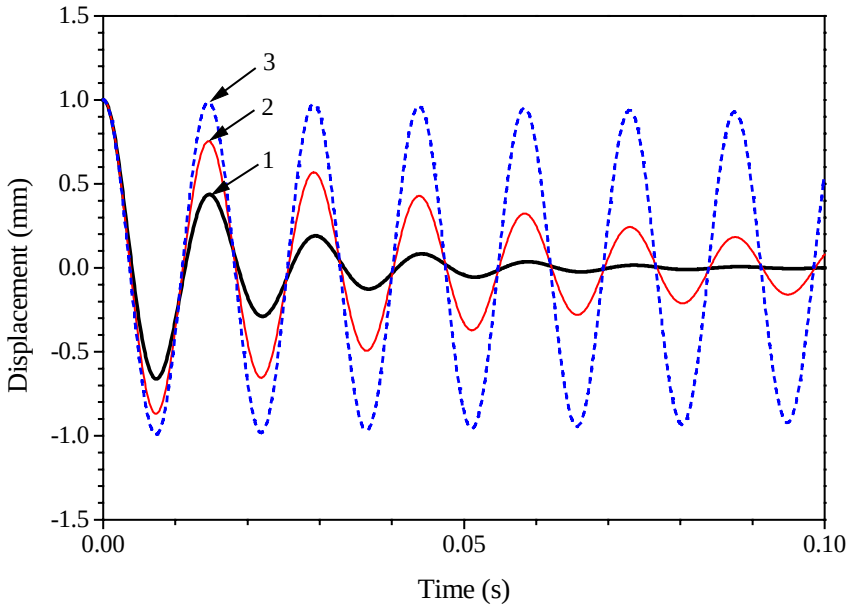

Fig. 8. Control with sensor/actuator at Location 3, $m = 3$: 1, optimal control ($\bar{\mathbf{G}}$); 2, control ($\mathbf{G}^*$); 3, free vibration; $\mathbf{G}^* = [200, 100]$, $\bar{\mathbf{G}} = [7.291031\text{E–}06, 299.678100]$, time step = 0.1 ms.

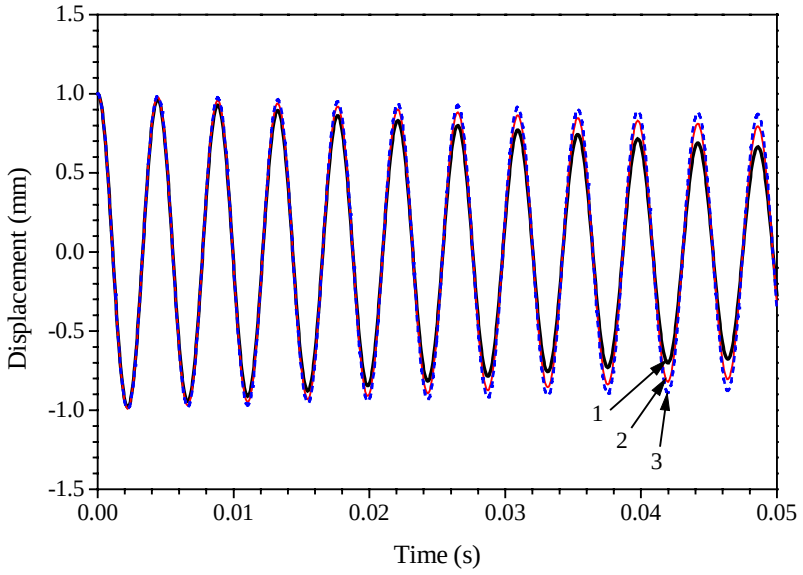

Fig. 9. Control with sensor/actuator at Location 1, $m = 4$: 1, optimal control ($\bar{\mathbf{G}}$); 2, control ($\mathbf{G}^*$); 3, free vibration; $\mathbf{G}^* = [200, 100]$, $\bar{\mathbf{G}} = [6.622339\text{E}{-}06, 299.149400]$, time step = 0.05 ms.

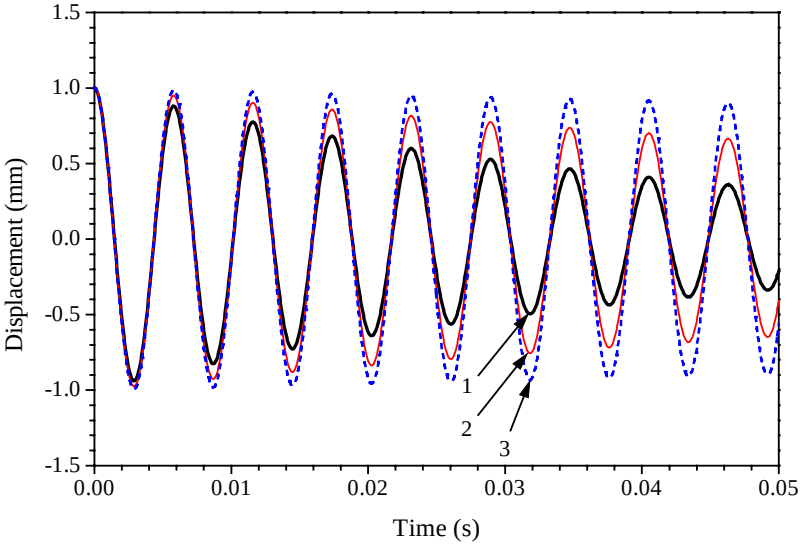

Fig. 10. Control with sensor/actuator at Location 2, $m = 4$: 1, optimal control ($\bar{\mathbf{G}}$); 2, control ($\mathbf{G}^*$); 3, free vibration; $\mathbf{G}^* = [200, 100]$, $\bar{\mathbf{G}} = [3.194133\text{E}{-}06, 299.614500]$, time step = 0.5 ms.

curvature of paraboloidal shells change with respect to shell locations, and these changes amplify the local characteristics resulting in frequency variations. Natural frequencies of the whole structure are usually the global average effect of all locations on the non-constant radii paraboloidal shell. These local/global phenomena were also observed in lab experiments [18].

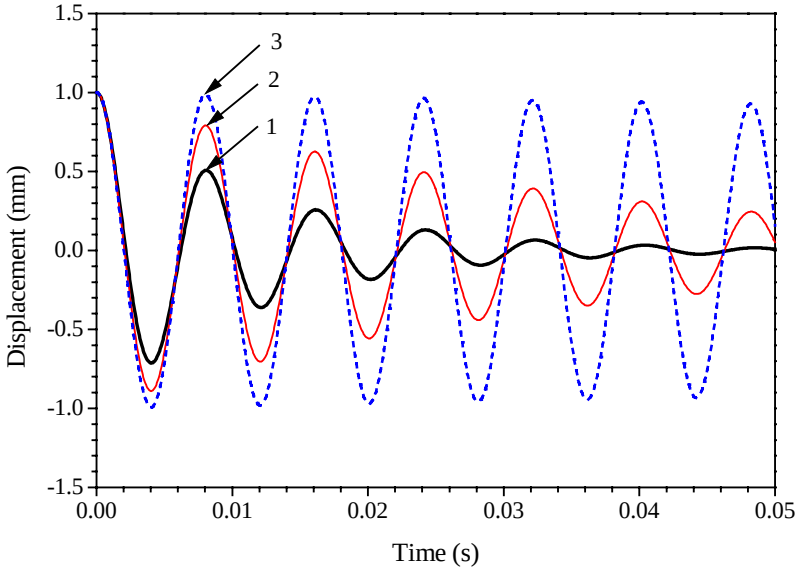

Fig. 11. Control with sensor/actuator at Location 3, $m = 4$: 1, optimal control ($\bar{\mathbf{G}}$); 2, control ($\mathbf{G}^*$); 3, free vibration; $\mathbf{G}^* = [200, 100]$, $\bar{\mathbf{G}} = [1.484552\text{E}{-}06, 299.465900]$, time step = 0.5 ms.

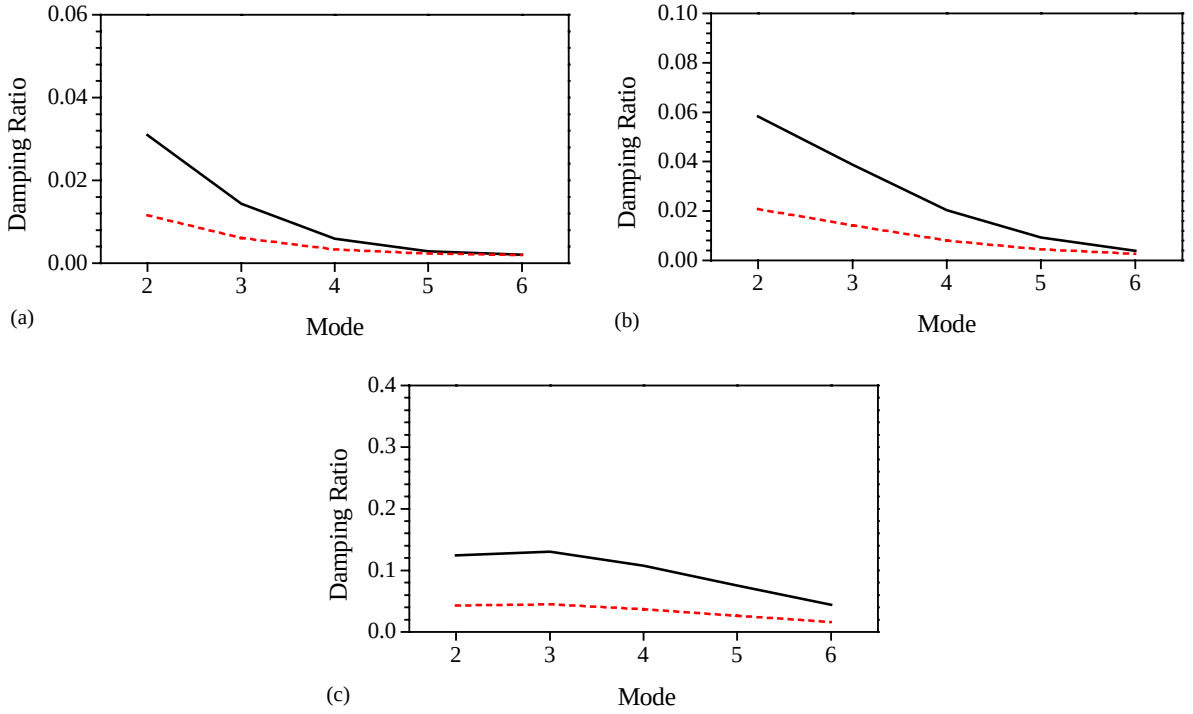

Fig. 12. Controlled damping ratio variation with the natural modes: —, optimal control ($\bar{\mathbf{G}}$); - - -, control ($\mathbf{G}^*$). (a) Location 1, (b) Location 2, (c) Location 3.

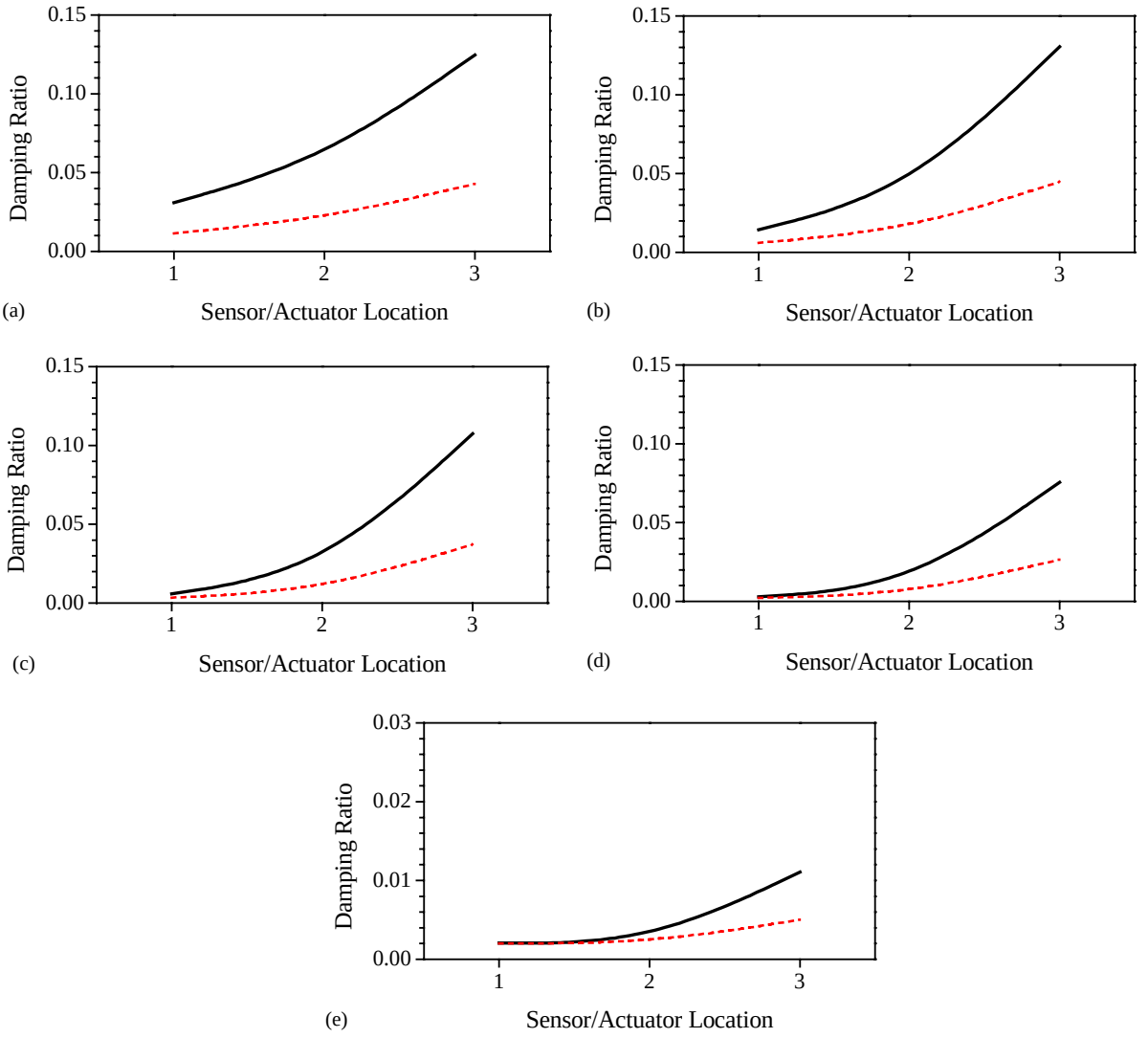

Fig. 13. Controlled damping ratio variation with locations: —, optimal control ($\bar{\mathbf{G}}$); - - -, control ($\mathbf{G}^*$). (a) $m = 2$, (b) $m = 3$, (c) $m = 4$, (d) $m = 5$, (e) $m = 6$.

These data suggest that the sensor/actuator patches near the free shell boundary generate better control results at the same control gain cost. The sensor/actuator patches near the shell boundary have larger sensing/actuating efficiency, besides the shell is also relatively flexible at the free boundary and thus, it is easier to control. The control effects of lower modes are better than those of higher modes at identical feedback gains; the controlled responses are almost unnoticeable at higher modes in some cases, due to low sensing/control signals. It is noted that the controlled damping ratio of the third mode ($m = 3$) is slightly larger than that of the second mode ($m = 2$) at Location 3 in Fig. 12(c). Earlier studies show that there are two modal-influenced contradictory

trends in the sensing signal and the open-loop control force characteristics of free-boundary paraboloidal structronic shells. The sensing efficiency increases with the increase of natural mode number, while the control efficiency decreases with the increase of mode number. That suggests that the best closed-loop control effect appears at certain medium modes rather than either the lowest or a much higher mode. A local frequency variation could also contribute to the modal-dependent control effect. To exclude the influence of frequency variation at different shell locations, the inferred damping ratios are calculated again using the global natural frequencies and the results suggest that (1) the best control effect is now the lowest mode $m = 2$; (2) the damping ratio differences among the three locations decrease; and (3) the influence of frequency variation to damping ratio is insignificant at the higher modes [16].

Note that comparing the control effort based on the control energy cost can be an alternative performance evaluation criterion, in which non-constant-cost tuned weightings can be used to achieve specified performances or outcomes (i.e., controlled damping ratios). In this case, the required energy to achieve similar outcomes would be modal dependent, since the in situ segmented sensor generates less sensing signal at higher natural modes. Accordingly, to achieve a similar outcome, the signal needs a high gain amplification (i.e., more energy) to reach the similar actuator voltage and consequently a similar control effect. In this study, on the other hand, the constant control-cost derived weightings are used and thus the actuator voltage varies, so the controlled modal damping ratios are used for comparison among various sensor/actuator locations and natural modes. The former is a goal oriented approach (i.e., comparing cost or energy for a specified performance) and the latter is a *cost* oriented approach (i.e., comparing controlled damping ratios at specified gain costs). Both approaches examine the control effectiveness from two different perspectives.

6. Conclusions

A structronic shell system is defined as an elastic shell bonded, embedded or laminated with active-material based sensors and actuators governed by either in situ or external control electronics. This study focuses on the optimal vibration control of paraboloidal shell structronic systems using the linear quadratic (LQ) optimal state feedback. A closed-loop paraboloidal shell structronic system consisting of distributed sensors/actuators and controller coupled with the elastic paraboloidal shell was defined first, followed by the state-space equation and the optimal control equation based on the LQ state feedback control. Control effects of the same-size sensor/actuator patches at different locations were studied and compared; modal control effects of different shell natural modes were also investigated. The gain matrix was estimated based on minimizing a performance criterion function. Optimal control effects were compared with controlled responses with other non-optimal PD control parameters at the same control energy cost.

Parametric studies demonstrate that the optimal control $\bar{\mathbf{G}}$ of paraboloidal shells with free boundary is, indeed, superior to the PD control $\mathbf{G}^*$ at the same control gain cost. Analysis of sensor/actuator location sensitivity suggests that the sensor/actuator patches placed near the free boundary rim provide the highest control effect of the free-floating paraboloidal shell. Its control

effectiveness is obvious for low shell modes and the sensor/actuator located near the free shell rim. This effectiveness becomes insignificant, regardless the control algorithms, for higher shell modes or the sensor/actuator located near the shell pole. This implies that the closed-loop control system for oscillations at higher modes is relatively insensitive to various gain matrices set at identical total gain cost. Accordingly, many system and design parameters, e.g., geometry/material properties, boundary conditions, sensor/actuator placements, feedback control algorithms, dominating vibration modes, frequency performance of control electronics, instruments/devices, etc., influencing the closed-loop control effect need to be considered in practical implementation of the closed-loop control of precision paraboloidal shell structronic systems.

Acknowledgements

This research is supported, in part, by a Grant (F49620-98-1-0467) from the Air Force Office of Scientific Research (Project manager: Brian Sanders). This support is gratefully acknowledged.

References

[1] A.P. Sage, *Optimum Systems Control*, Prentice-Hall, Englewood Cliffs, NJ, 1968, pp. 137–164.
[2] V. Komkov, *Optimal Control Theory for the Damping of Vibration of Simple Elastic Systems*, Springer, Berlin, 1972.
[3] K. Nonami, Control performances based on control system design strategies for active structural control, *JSME International Journal, Series C* 38 (3) (1995) 367–378.
[4] M.C. Ray, Optimal control of laminated plate with piezoelectric sensor and actuator layers, *American Institute of Aeronautics and Astronautics Journal* 36 (12) (1998) 2204–2208.
[5] B. Fariborzi, Design of LQ and LC optimal controllers for plate vibration, in: H. Tzou, M.F. Golnaraghi, C.J. Radcliffe (Eds.), *Control of Vibration and Noise: New Milennium*, ASME, New York, 2000, pp. 33–145.
[6] Y.K. Lin, F.A. Lee, Vibrations of thin paraboloidal shells of revolution, *Journal of Applied Mechanics* 27 (1960) 743–744.
[7] J.T.S. Wang, C. Lin, On the differential equations of the axisymmetric vibration of paraboloidal shells of revolution, NASA CR-932, November 1967.
[8] H.S. Tzou, *Piezoelectric Shells (Distributed Sensing and Control of Continua)*, Kluwer Academic Publishers, Boston, 1993.
[9] J. Qiu, J. Tani, Vibration control of a cylindrical shell using distributed piezoelectric sensors and actuators, *Journal of Intelligent Material Systems and Structures* 6 (4) (1995) 474–481.
[10] H.S. Tzou, Y. Bao, Parametric study of segmented transducers laminated on cylindrical shells, Part 1: sensor patches, *Journal of Sound and Vibration* 197 (2) (1996) 207–224.
[11] H.S. Tzou, D.W. Wang, Distributed dynamic signal analysis of piezoelectric laminated linear and nonlinear toroidal shells, *Journal of Sound and Vibration* 254 (2) (2002) 203–218.
[12] *Symposium on Advances of Solids and Structures (PVP-8), ASME International Mechanical Engineering Congress*, New Orleans, LA, November 17–22, 2002, paper no. IMECE2002-32322.
[13] H.S. Tzou, J.H. Ding, Precision actuation effectiveness of segmented actuators laminated on paraboloidal reflectors, *Symposium on Active Control of Vibration and Noise, 2001 ASME International Mechanical Engineering Congress*, New York, November 12–17, 2001.
[14] H.S. Tzou, J.H. Ding, J. Hagiwara, Micro-control actions of segmented actuator patches laminated on deep paraboloidal shells, *JSME International Journal, Series C* 45(1) (2002).

[15] W. Soedel, *Vibrations of Shells and Plates*, Marcel Dekker, New York and Basel, 1981, pp. 47–50, 124–136.
[16] J.H. Ding, Micro-piezothermoelastic Behavior and Distributed Sensing/Control of Nonlinear Structronic Beam and Paraboloidal Shell Systems, Ph.D. Dissertation, University of Kentucky, 2002, pp. 394–396.
[17] B. Friedland, *Control System Design—An Introduction to State-space Methods*, McGraw-Hill, New York, 1986, pp. 59–63, 337–350.
[18] P.G. Glockner, K.Z. Tawardros, Experiments on free vibration of shells of revolution, *Experimental Mechanics* 13 (10) (1973) 411–421.